Prediction of flexoelectricity in $BaTiO_3$ using molecular dynamics simulations

Long Zhou(周龙)[1], Xu-Long Zhang(张旭龙)[1], Yu-Ying Cao(曹玉莹)[1], Fu Zheng(郑富)[1], Hua Gao(高华)[1], Hong-Fei Liu(刘红飞)[1], and Zhi Ma(马治)[1,2,†]

[1] *School of Physics and Electronic-Electrical Engineering, Ningxia University, Yinchuan* 750021, *China*
[2] *State Key Laboratory of High-Efficiency Utilization of Coal and Green Chemical Engineering, Ningxia University, Yinchuan* 750021, *China*

(Received 9 February 2022; revised manuscript received 5 April 2022; accepted manuscript online 18 May 2022)

Flexoelectric effect, referring to the strain gradient induced polarization, widely exists in dielectric materials, but its molecular dynamics has not been studied so much so far. In this work, the radial distribution function of $BaTiO_3$ and the phase transition temperatures have been investigated, and the results show that the core-shell potential model is effective and the structure of $BaTiO_3$ is stable in a temperature range of 10 K–150 K. Molecular dynamics simulated hysteresis loops of $BaTiO_3$ show that anisotropy can play an important role in the coercive field. Based on the rational simulation process, the effects of cantilever beam bent angle and fixed length on the polarization are analyzed. It is found that the small bent angle of the curved cantilever beam can give a proportional relationship with a fixed end length and a non-linear relationship is presented when the bent angle is much larger. The prediction of flexoelectric coefficient in $BaTiO_3$ is 18.5 nC/m. This work provides a computational framework for the study of flexoelectric effect by using molecular dynamics.

Keywords: flexoelectric effect, molecular dynamics, phase transition, hysteresis loop

PACS: 77.65.Ly, 02.70.Ns, 05.70.Fh, 75.60.Ej **DOI:** 10.1088/1674-1056/ac70be

1. Introduction

With the rapid development of science and technology, smart devices are becoming ever more intelligent and portable, but the size of the device is to be smaller and smaller. Recently, nanogenerators,[1] nanocapacitors, energy harvesters,[2,3] and actuators are considered to be very promising technologies, in which flexoelectric effect will play a key role. So the larger flexoelectric effect is desired. A new method of measuring flexoelectric response on freestanding cantilever beams by using nanoindentation instrumentation has been presented.[4] The measured flexoelectric response of ferroelectric ceramics is usually several orders of magnitude larger than the theoretically calculated response.[5] Flexoelectricity has aroused more and more interest due to the fact that flexoelectricity is the fourth rank tensor and appliable for nano-scale devices under certain conditions.

Normally, the flexoelectric effect occurs in nonuniformly deformed dielectrics and the deformation induced polarization is usually proportional to the strain gradient. Since the strain gradient can break the inversion symmetry of even a centrosymmetric crystal, flexoelectricity even exists in non-piezoelectric material. So the flexoelectric effect is possible to occur in dielectrics of any symmetry. It has a wider scope of applications. Thus, the flexoelectric effect plays an important role in describing the interaction between elastic strain and free electrons in a non-piezoelectric crystal. When the deformation of the dielectric can be made very large in the sense of nanoscale, the polarization caused by the flexoelectric effect becomes more obvious and therefore it will have a practical value and diverse applications.

In the early stage of research on flexoelectric effect, all earlier investigators agreed that the effect is tiny in simple crystalline dielectrics. The flexoelectric coefficient is relatively small, about 10^{-9} C/m.[6] Later, Ma and Cross[7–9] obtained large flexoelectric coefficients of some piezoelectric materials through a series of experimental tests, and they reported that the flexoelectric coefficient of barium strontium titanate (BST) can reach 10^{-4} C/m, which is five orders of magnitude higher than the theoretically predicted value. However, the microscopic mechanism and macroscopic mechanism of the extremely large flexoelectric effect are still not clear.

With the development of computer technology, the theoretical calculation of flexoelectric effects has achieved a breakthrough in this century. Maranganti and Harma developed core–shell modeling methods to perform *ab initio* calculations for the flexoelectric coefficients in some semiconductor materials.[10] The first-principles calculated flexoelectric coefficient is between 10^{-8} C/m and 10^{-10} C/m, which is basically consistent with the theoretical value,[11,33] generally much smaller than the experimental measurement. This discrepancy between experimental result and theoretical result remains unexplained to date.

In fact, there are many difficulties in accurately measuring the flexoelectric coefficient. Recently, two approaches to

[†]Corresponding author. E-mail: mazhi@nxu.edu.cn

© 2023 Chinese Physical Society and IOP Publishing Ltd

measuring the flexoelectric parameters were developed: one is a cantilevered beam based dynamic approach and the other is an approach based on static measurement by using several-point bending fixtures. The point bending is more popular. However, for the cause of the brittleness, the deformation of the dielectric sample cannot be made much larger. The flexoelectric coefficients can only be determined from a few small bending cases. On the other hand, the flexoelectric coefficient of the bending strip is usually obtained under the condition of a certain fixed length. As is well known, the longer the free length of the sample, the greater the generated strain gradient will be. Thus when the flexoelectric coefficient is determined, the effect of this factor cannot be ignored, either.

Barium titanate ($BaTiO_3$) is part of the most widely investigated perovskite-type ferroelectrics and possesses many technological applications. Either in theory or in experiment/simulations, $BaTiO_3$ is really a much better model for comparative research. In this work, we consider the influences of different loading conditions on the flexoelectric coefficient of $BaTiO_3$ and propose a general method of predicting the flexoelectric coefficient. Since much physical infromation cab be obtained from molecular dynamics simulation on a nanoscale and a relatively continuous strain gradient can be made to extremely large, it is believed that the predicted flexoelectric coefficient from this method is more accurate, and the effect of bending angle on the flexoelectric coefficient can be fully revealed.

2. Theory and methodology

In classical molecular dynamics, each molecule is considered as a point mass and Newton's equations are integrated to compute their motion. From the motion of the ensemble, it can extract a variety of useful microscopic and macroscopic information. It contains all the physics of the model system in a potential function from which the individual force equations can be derived for each atom. In this work, the molecular dynamics method is used through LAMMPS.[12,13] The model employed in the simulation is the adiabatic core–shell model proposed by Mitchell and Fincham.[14] The schematic diagram of the core–shell model is presented in Fig. 1. And it takes the interaction potential parameters used from the core–shell model potential function developed by Sepliarsky *et al.*,[15] which are summarized in Table 1. The core–shell model is widely used in the simulation of perovskite oxides because it can consider both ion polarization and electronic polarization. The core–shell model is composed of a positively charged core and a negatively charged shell. Since the shell is massless, the shell is very sensitive to the movement of the core. During the simulation, one way is to assign a small mass to the shell to make the shell and core have a similar movement. It has proven this method effective in numerous researches.[14–16]

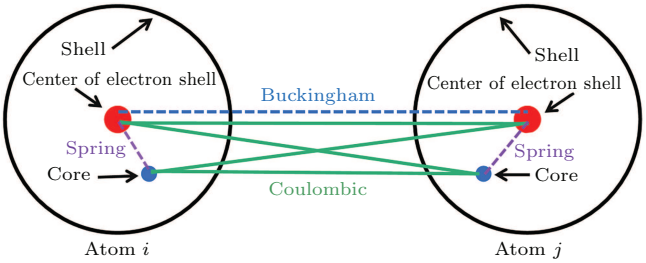


Fig. 1. Schematic diagram of core–shell model, which is composed of a positively charged core and a negatively charged shell.

Table 1. Parameters for core–shell model of $BaTiO_3$ ferroelectrics.[15]

Atoms	Core charge $\|q_i\|$	Shell charge $\|q_j\|$	k_2 (eV/Å^2)	k_4 (eV/Å^4)	Buckingham			
						A (eV)	ρ (Å)	C (eV/Å^6)
Ba	5.62	–3.76	251.8	0.0	Ba–O	1061.30	0.3740	0.0
Ti	4.76	–1.58	322.0	500.0	Ti–O	3769.93	0.2589	0.0
O	0.91	–2.59	31.0	4000.0	O–O	4740.00	0.2686	160.0

The interaction potential of $BaTiO_3$ core–shell model comprises three parts. The first part is the potential that is the short-range interaction between shell–shell and described by Buckingham potential. Buckingham potential reflects the repulsive force and van der Waals gravitation between shell–shell. The formula is as follows:

$$V_{r_{ij}}^{\mathrm{Buck}} = A\exp\left(-\frac{|r_{ij}|}{\rho}\right) - \frac{C}{r_{ij}^6}. \tag{1}$$

Here, r_{ij} is the distance between two core–cores, and A, ρ, and C are the parameters of the potential. The second part is the potential that is the Coulomb potential, which considers the long-range electrostatic interaction between two particles. The Coulomb potential reflects the core–shell interaction between different particles. The potential is

$$V_{r_{ij}}^{\mathrm{Coulomb}} = \frac{q_i q_j}{4\pi\varepsilon_0 |r_{ij}|}. \tag{2}$$

Here, q_i and q_j are the charge of particles i and j, ε_0 is the vacuum permittivity. The third part is the interaction between the core–shells of the same atom. The interaction between the core and the shell of an atom is treated exclusively as anharmonic spring with the potential parameters k_2 and k_4. The formula is written as

$$V_{r_{ij}}^{\mathrm{Spring}} = \frac{1}{2}k_2|r_{ij}^2| + \frac{1}{24}k_4|r_{ij}^4|. \tag{3}$$

Classical molecular dynamics is a useful computational tool for simulating the properties of liquids, solids, and molecules. From the motion of the ensemble of atoms, it can extract structural or conformational properties from the simulation process. In studying the radial distribution function, the phase transition and its behavior under an applied electric field can be obtained. A size of $10\times10\times10$ supercell, which consists of 10000 atoms, is established. Both the periodic boundary conditions and the conjugate gradient method are used in this simulation. This method needs a small amount of storage, has step convergence and high stability, and requires no external parameters. All the equilibrium processes of molecular dynamics simulation use the NPT ensemble. The pressure control method adopts Nose–Hoover pressure control, and the damping parameter is 0.4. Unlike the equilibrium process, the NVE ensemble is chosen for the calculations of flexoelectric effect and the radial distribution function . Because of the high vibration frequency of the shell, we adopt a time step of 0.4 fs, which is enough small for the entire simulation process. In addition, when the flexoelectric effect of $BaTiO_3$ is studied, a cantilever beam structure with a size of $64\times8\times8$ supercell is established, which consists of 40960 atoms. One end of the cantilever beam is fixed, and then a downward (as Y direction) force is exerted on the other end. After continuous testing, we impose periodic boundary conditions in the Z direction, non-periodic ones in the X direction, and shrink-wrapped boundary condition in the Y direction.

3. Results and discussion

3.1. Radial distribution function

The radial distribution function $g(r)$ is used to describe the distribution of the distance between atoms in the system.[17,18] At the distance r from the fixed atom, the average number of atoms in the shell with the width $\mathrm{d}r$ is denoted as $n(r)$. In the method of calculating $n(r)$, all atoms in the system are regarded as solid atoms, thus the $n(r)$ of each solid atom can be calculated, and finally the mean value is obtained. If the atoms in the system are evenly distributed, the ratio of $n(r)$ to the total number of atoms in the shell is described as the radial distribution function $g(r)$ below:

$$g(r) = \frac{V}{N4\pi r^2 \mathrm{d}r} n(r), \tag{4}$$

where $g(r)$ depends on the structure of the crystal. For an ideal crystal, $g(r)$ has an infinitely tall peak at a certain distance.

In order to better understand the stability of the established $BaTiO_3$ model and its microscopic behaviors at different temperatures, the radial distribution functions (RDFs) of $BaTiO_3$ with an $R3m$ phase structure are calculated at four different temperatures of 10 K, 50 K, 100 K, and 150 K, respectively.

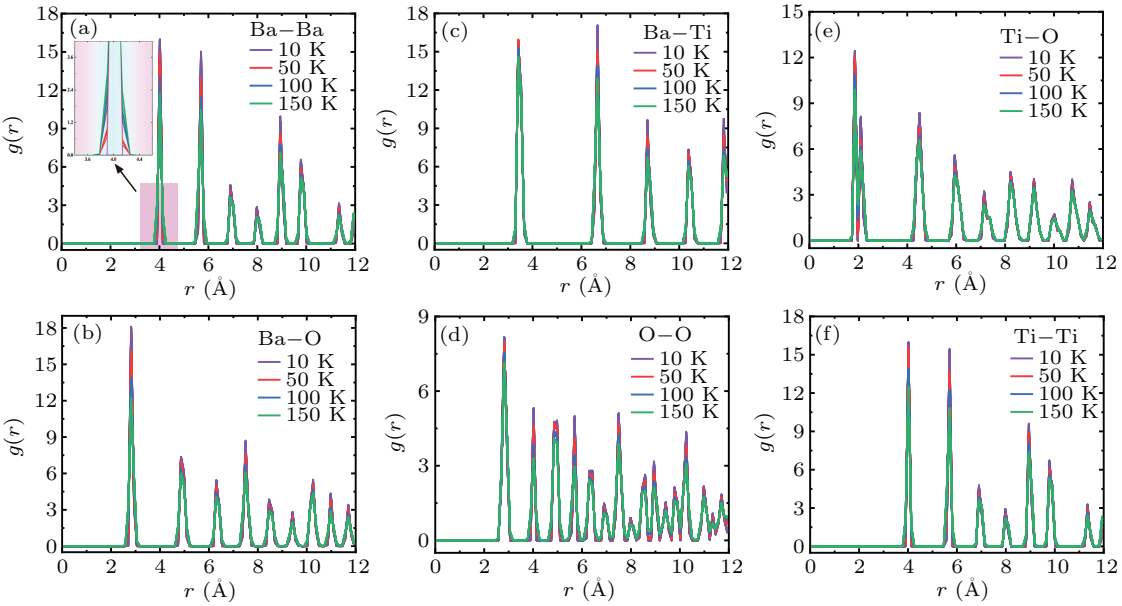


Fig. 2. RDF plots of $BaTiO_3$ at temperatures of 10 K, 50 K, 100 K, and 150 K, with radial distribution function $g(r)$ calculated between atoms (a) Ba–Ba, (b) Ba–O, (c) Ba–Ti, (d) O–O, (e) Ti–O, and (f) Ti–Ti.

It can be seen from Fig. 2 that the radial distribution function shows sharp peaks at temperatures of 10 K, 50 K,100 K, and 150 K. Figures 2(a)–2(f) show the calculated RDF $g(r)$ between atoms Ba–Ba, Ba–O, Ba–Ti, O–O, Ti–O, and Ti–Ti respectively. These peaks indicate that the atoms of the system are closely packed. By comparing the RDF of the pairs atoms at different temperatures, it can be found that the higher the temperature, the smaller the $g(r)$ value is and the wider the peak width (see the inset in Fig. 2(a)). Because when the temperature rises, the crystal lattice vibration becomes more active. In addition, the RDF can also indicate the distance between the pairs atoms. For example, the first peak of the Ba–Ba RDF is located at 4.02 Å, which can be interpreted as the bond length of Ba–Ba. Table 2 shows the interatomic dis-

tance and the first coordination numbers of $BaTiO_3$ at 10 K, 50 K, 100 K, and 150 K. The result of the coordination number is verified by its perovskite structure. The coordination numbers of $BaTiO_3$ remains unchanged at the three temperatures, which explains that $BaTiO_3$ is stable in the temperature range of 10 K–150 K. The results of this molecular dynamics simulation illustrate that the basis/primitive crystal does not change with temperature.

Table 2. Interatomic separations and first coordination numbers of $BaTiO_3$ at 10 K, 50 K, 100 K, and 150 K.

Pair	Interatomic separation/bond length (Å)				First coordination number			
	10 K	50 K	100 K	150 K	10 K	50 K	100 K	150 K
Ba–Ba	4.02	4.02	4.02	4.02	6	6	6	6
Ba–Ti	3.42	3.42	3.42	3.42	8	8	8	8
Ba–O	2.82	2.82	2.82	2.82	12	12	12	12
Ti–Ti	4.02	4.02	4.02	4.02	6	6	6	6
Ti–O	1.86	1.86	1.86	1.86	6	6	6	6
O–O	2.82	2.82	2.82	2.82	8	8	8	8

3.2. Phase transition

$BaTiO_3$ always has diverse phase transitions in a wide temperature range. To further verify the correctness and validity of the core–shell potential function, the phase transition of $BaTiO_3$ is investigated. It established rhombohedral phase $BaTiO_3$ as an initial structure. The lattice constant is 4.016 Å, the tilt angle is 89.67°, and the initial size of the model is $10\times10\times10$, where 10 is the number of unit cells along each side of the simulation box. The time step of the simulation process is 0.4 fs, the temperature increases from 10 K to 460 K within 5×10^5 steps. The simulated results are displayed in Fig. 3.

From Fig. 3 it can be seen that the molecular dynamics simulation with the core–shell potential can correctly reproduce the three phase transitions of $BaTiO_3$: rhombohedral → orthorhombic → tetragonal → cubic. In Fig. 3, the dashed line divides the area into different phase ranges, where R, O, T, and C in the figure denote the rhombohedral, orthorhombic, tetragonal, and cubic phases, respectively. The calculated $BaTiO_3$ phase transition temperatures are listed in Table 3. Figure 3(a) shows the variation of polarization with temperature, which is similar to that of lattice parameter in Fig. 3(b). It is shown that the lattice parameters with various symmetries increase as temperature increases, but the basis/primitive $BaTiO_3$ phase remains even unchanged in the temperature range of 10 K–150 K (As shown in Table 2). These results are in agreement with those reported in the literature.[19] This phenomenon reveals that the distortion of the crystal lattice is one of the most important reasons for the change in the polarization properties of the crystal.

For comparison between different research methods, the phase transition results are divided into three categories. The first category is to study the phase transition temperature of $BaTiO_3$ by using molecular dynamics method. We can see that the same method is used, but the results are different. The reason for this difference may be that the parameter settings are different, such as pressure, damping parameters, heating rate, etc. In addition, Luis's research shows that the size effect is also an important influencing factor. The second category is the experimental results. Obviously, compared with other MD results, except that the phase transition temperature of O→T is slightly lower than the experimental value, our research results are very close to the experimental values. The third category is the $BaTiO_3$ phase transition temperature obtained by Cross[26] through Landau theory. Compared with the Cross's research results, except that the phase transition temperature of T→C is close to the Cross's result, the other two phase transition temperatures are lower than the Cross's research results but near the experimental values.

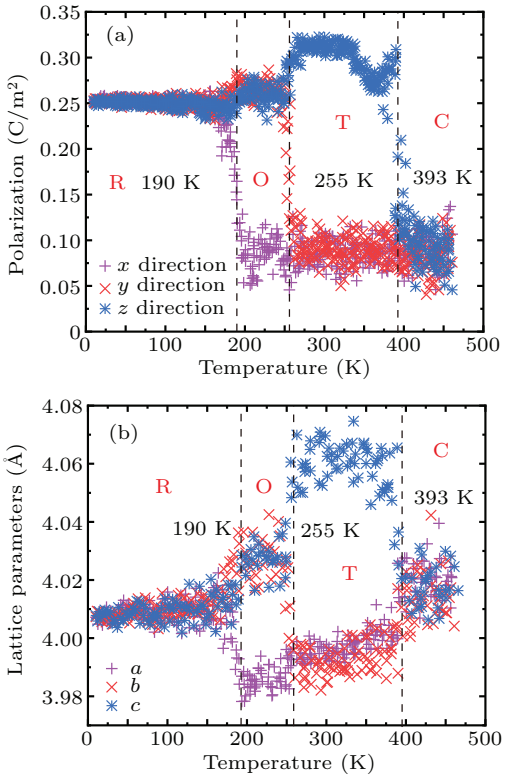


Fig. 3. $BaTiO_3$ phase transitions at temperatures ranging from 10 K to 460 K, showing (a) polarization intensity with temperature, and (b) lattice parameters with temperature, where dashed line denotes phase transition temperature value and R, O, T, and C denote rhombohedral, orthorhombic, tetragonal, and cubic phases, respectively.

Table 3. Comparison among $BaTiO_3$ transition temperatures.

Phase transition	MD study			Experimental value		Landau theory
Temperature (K)	This study	Luis[20]	Tinte[21]	Lemanov[22]	Merz[23]	Bell[24]
R→O	190	207	140	183	178–202	202
O→T	255	254	190	278	268	281
T→C	393	410	360	393	393	398

3.3. Hysteresis loop

Indeed, the polarizations in perovskites can be induced by the temperature or an external electric field or a stress field. To investigate the anisotropy of rhombohedral $BaTiO_3$ under an applied electric field, an electric field of up to 180 MV/m is applied in three directions [001], [110], and [111] separately. Owing to the effect of anisotropy, some hysteresis loops are saturated under the maximum applied field, while others often do not. The simulated hysteresis loops of $BaTiO_3$ crystal are shown in Fig. 4.

Figures 4(a)–4(c) show the polarizations of $BaTiO_3$ in three directions [001], [110], and [111] at 100 K, respectively. It is found that the hysteresis loop along the [111] direction is saturated under the maximum applied field, but not in other directions. Experimentally, the measured hysteresis loops are usually difficult to reach a saturated level due to the presence of the breakdown field. This phenomenon makes it very difficult to determine the intrinsic parameters of the ferroelectric samples. Eventually, a new model of polarization-electric field hysteresis loops is derived mathematically by Ma *et al*. The external energy such as the temperature field and the stress-strain field have been analyzed as an energetic parameter synthetically in this model.[25]

$$P = P_{\mathrm{S}} \frac{\sinh(U \cdot E_{\mathrm{app}} \pm U \cdot E_{\mathrm{C}})}{P_{\mathrm{S}} \cdot U/\chi - 1 + \cosh(U \cdot E_{\mathrm{app}} \pm U \cdot E_{\mathrm{C}})}, \tag{5}$$

where P is polarization.Thereout, the ferroelectric intrinsic parameters can be calculated directly by the geometric shapes of hysteresis loop. This model implies that the hysteresis loop of ferroelectric material can be determined by four parameters: the saturation of polarization P_{S}, the coercive field E_{C}, the electric susceptibility χ, and the equivalent energy U. In Table 4 listed are the fitted intrinsic parameters provided by Eq. (5). It can be observed that under the same applied maximum electric field, coercive field is significantly different, but the intensity of their saturation polarization varies very little. This result demonstrates that anisotropy can have an important effect on the structure and motion of ferroelectric domains, but not on saturation polarization.

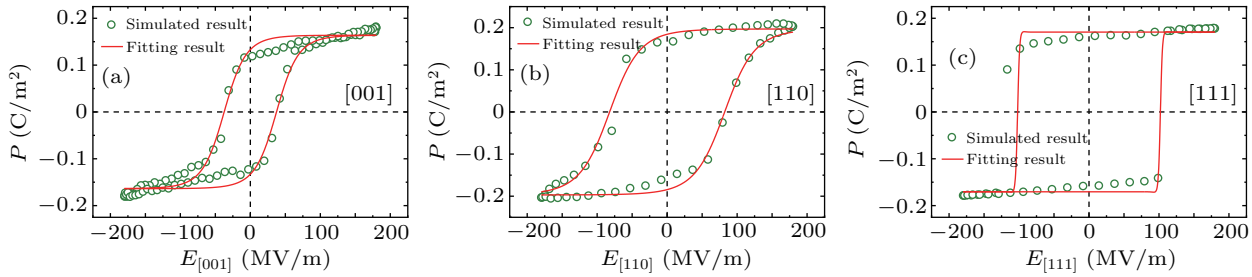


Fig. 4. Simulated hysteresis loops of $BaTiO_3$ in three directions of (a) [001], (b) [110], and (c) [111], where discrete data points are from molecular dynamics simulations, while the lines are obtained from theoretical model of hysteresis loop.

Table 4. $BaTiO_3$ intrinsic parameters from fitting of hysteresis loops.

	P_{S} (C·m^{-2})	χ (C·MV^{-1}·m^{-1})	U (C·m^{-2})	E_{C} (MV·m^{-1})
[001]	0.1638	0.0052	0.0428	37.3988
[110]	0.1969	0.0045	0.0310	82.2178
[111]	0.1705	0.0602	0.3183	102.0427

3.4. Flexoelectric effect

Flexoelectric effect is a property of a dielectric material, its mechanism is that the strain gradient breaks the spatial inversion symmetry inside the dielectric material, so that the center of positive changes and negative charges no longer overlap with each other and their polarizations occur whereby exhibiting an electrical polarization induced by a strain gradient. Flexoelectricity is closely related to piezoelectricity. The piezoelectric effect is limited to non-centrosymmetric materials, whereas flexoelectric effect is universal in all dielectrics. Flexoelectric effect is significant due to larger strain gradients on a nanoscale. Ma and Cross studied the flexoelectric properties of high-dielectric ceramics such as barium strontium titanate (BST), lead zirconate titanate (PZT), and lead magnesium niobate (PMN) experimentally. The flexoelectric effect in flexible materials is very significant, and the flexoelectric coefficient reaches 10^{-6} C/m.[7–9,26] Maranganti and Sharma calculated the flexoelectric coefficient to be about 10^{-9} C/m[27] through the first-principles method. The first-principles calculated value of the flexoelectric coefficient is usually between 10^{-8} C/m and 10^{-10} C/m, which is basically consistent with the theoretical calculations of Pikin and

Indenbom.[28]

The molecular dynamics method can simulate the flexoelectric effect of the dielectric material at a large angle, which is difficult to achieve experimentally. The simulation process can continuously change the bending angle, which is also problematic in the experiment that only a few small angles can be measured. In general, the positive flexoelectric effect is studied by flexoelectric coefficient μ_{ijkl}, which is a fourth-order tensor. The mathematical form of positive flexoelectric effect is[26,29]

$$P_i = \mu_{ijkl}\frac{\partial S_{jk}}{\partial x_l}. \tag{6}$$

For the convenience of description, the four subscripts of flexoelectric coefficient μ_{ijkl} can be omitted.[26,30] It is believed that the flexoelectric coefficient and the electrostriction coefficient have the same symmetry. The electrostriction coefficient is generally expressed as[26]

$$S_{ij} = Q_{ijkl}P_kP_l. \tag{7}$$

Therefore, taking μ_{ijkl} under a cubic crystal for example, μ_{ijkl} has a total of 3 non-zero independent components, namely μ_{11}, μ_{12}, and μ_{44}, where μ_{11} refers to the longitudinal coefficient, μ_{12} the transverse coefficient, and μ_{44} the shear coefficient.[31]

The key to calculating the flexoelectric coefficient is how to calculate the strain gradient. According to the strain gradient of the cantilever beam model, its schematic diagram is shown in Fig. 5.

As shown in Fig. 5, after the cantilever beam is deformed, the coordinates of the top right corner vertex change from (X_0, 0) to point $M(P,Q)$, the thickness of the cantilever beam is known to be Y_0, the full length of the cantilever beam is X_0, and the bent cantilever beam can be regarded as a small segment of a circle with radius R, where α is the angle corresponding to the small arc. The position coordinates of the upper right vertex $M(P,Q)$ of the cantilever beam after bending are as follows:

$$P(X,Y) = R\sin(\alpha), \tag{8}$$

$$Q(X,Y) = R - R\cos(\alpha). \tag{9}$$

The strain gradient can be obtained from the following equation:[32]

$$\frac{\partial S_{11}}{\partial Y} = R\left(\frac{\alpha}{X_0}\right)^2. \tag{10}$$

When the bending of a cantilever beam becomes greater, this bent cantilever beam can be regarded as a segment of a circle arc as shown in Fig. 6. It is assumed that β is the angle corresponding to a circle arc.

It can be seen from Fig. 6, if it l is assumed to be the distance from point M to the y axis and d the distance from point M to the x axis, the expression of l and d are respectively

$$l = R\sin(\beta), \tag{11}$$

$$d = R - R\cos(\beta). \tag{12}$$

Combining the two equations above, the ultimate expression of R and β are

$$\beta = \arccos\left(\frac{l^2 - d^2}{l^2 + d^2}\right), \tag{13}$$

$$R = \frac{l^2 + d^2}{2d}. \tag{14}$$

Since the value of l and d can be calculated from the atom position at M point, the strain gradient can be calculated. In this work, a $64 \times 8 \times 8$ cell model with a total of 40960 atoms is built. And in the x direction, the model consists of three parts: the fixed part, the free part, and the forced part. The fixed part refers to grouping a certain number of cells into a group at the left end of the model, and all the atoms in this group are fixed so as to achieve the effect of fixing one end of the cantilever beam and bending the other end. The relaxing part refers to the middle part of the cantilever beam. Cells are grouped, and they are not subjected to force in the entire simulation process, and can be changed freely in the entire simulation process. The forced part is set up at the right end of the model, and it has applied a downward force to this group of atoms to make the cantilever beam bent.

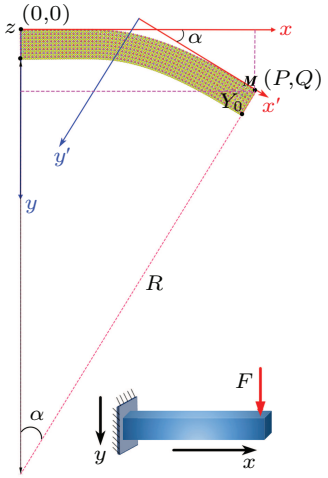


Fig. 5. Cantilever beam bending diagram, with lower right corner illuminating the direction of applied force in y direction, and α denoting the angle between the end of the bending beam and the horizontal axis.

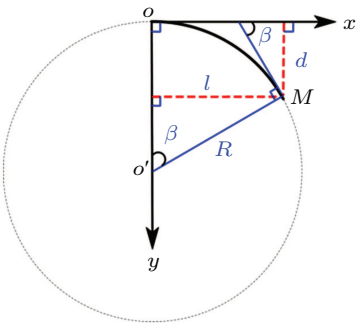


Fig. 6. Bent cantilever beam regarded as a segment of circle arc, with l denoting the distance from point M to the y axis and d the distance from point M to x axis.

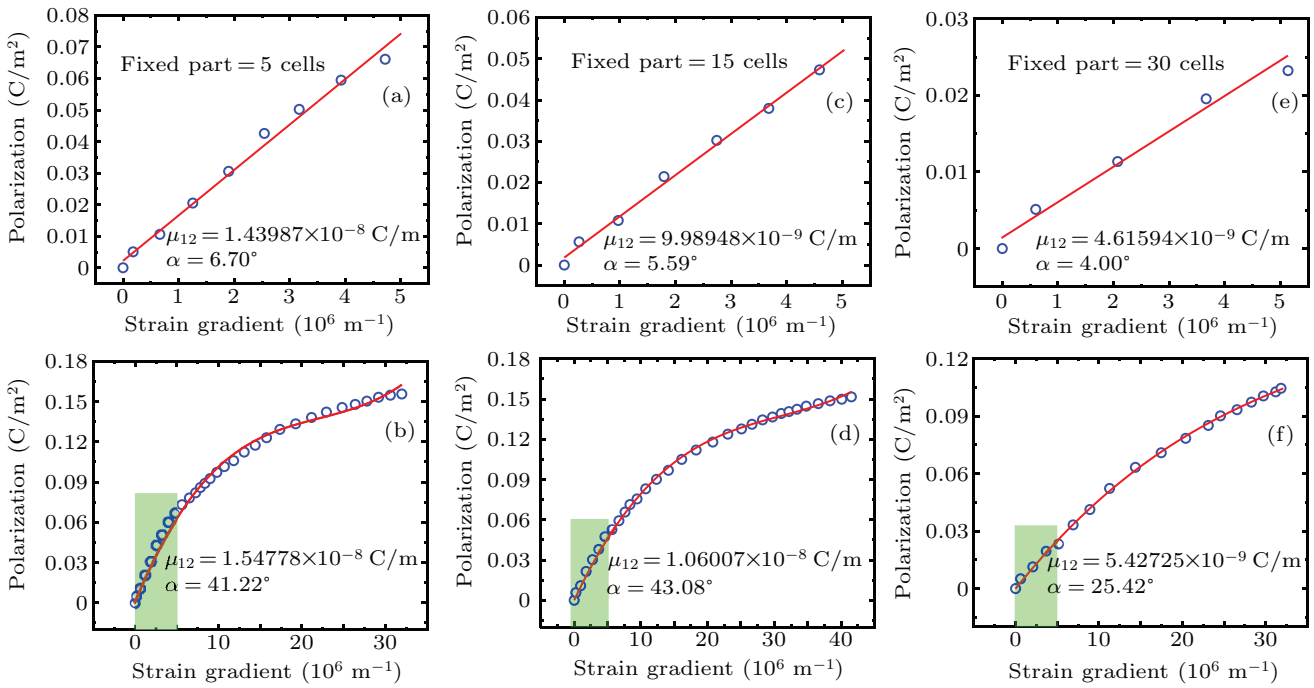


Fig. 7. Small angle and large angle bendings at different fixed lengths of cantilever beam. Each upper panel shows the analyses of part of plot (marked by shade area) on its corresponding lower panel. The length of the fixed part is (a)–(b) 5 cells, (c)–(d) 15 cells, and (e)–(f) 30 cells, separately.

Owing to the fact that flexoelectric effect is related to the curvature of the cantilever beam, the effects of different lengths of the fixed end on the flexoelectric coefficient of $BaTiO_3$ are investigated. During the simulation, a constant downward force of 0.05 kPa is exerted on the forced part. The entire simulation is performed at a temperature of 10 K, the conjugate gradient method is used to minimize the energy, and the time step is 0.4 fs. By changing the length of the fixed end to obtain different angles of bending, the length of the fixed part increases continuously from 5 cells to 8 cells, 10 cells, 13 cells, 15 cells, 18 cells, 20 cells, 23 cells, 25 cells, 28 cells, and 30 cells. All the small angle bendings and larger angle bendings are investigated and to not be cumbersome the plots in Fig. 7 are only for samples with fixed 5 cells, 15 cells, and 30 cells.

In Fig. 7, the plots in the first row show the results for a small angle bending, corresponding to the marked shaded box of a large angle bending in the second row. It is determined that they exhibit distinct regularities, the former part presents a linear relationship while the latter part is non-linear. So it controls the upper plots with linear fitting in the smaller angle range within 7°, which is consistent with the experimental result. For the flexoelectric coefficients generated by the large-angle bending as shown in Fig. 7 in the bottom row, a third-order polynomial is used to fit the plot. The flexoelectric coefficients obtained by the two fittings are marked, and the maximum bending angle is also marked. The maximum bent angle is close to 44°. We can see it from these two rows that the small-angle bending flexoelectric coefficient maintains a good linear relationship with the strain gradient, while the large-angle bending has a nonlinear effect. In order to compare the linear effect with the nonlinear effect, we draw the obtained maximum flexoelectric coefficient in Fig. 8.

Figure 8(a) shows the variation of the flexoelectric coefficient of the linear effect and the nonlinear effect on the length of the fixed cantilever beam end. It can be seen from the figure that the flexoelectric coefficient gradually decreases with the length of the fixed end increasing, but the nonlinear flexoelectric coefficient produced by larger bending is obviously greater than the linear one. Therefore, the magnitude of the flexoelectric coefficient is closely related to the length of the fixed part or the angle of the cantilever beam bending. The two sets of flexoelectric coefficients versus fixed length are shown in Fig. 8(b), and a linear fit to the small angle bending is performed, then the intercept can be obtained by the linear fitting. The intercept is the theoretically obtainable maximum flexoelectric coefficient. This linear relationship can be consulted in the following analysis. When the bending angle is much smaller, $l \approx R \cdot \beta$, the bending length l is much closer to the initially bent cantilever beam length $L - x$, so, flexoelectric coefficient can be obtained from the following equation:

$$\mu \approx \frac{P}{\beta} \cdot (L - x), \tag{15}$$

where L is the whole cantilever beam length, P is the polarization, and x is the fixed length. It indicates that the flexoelectric coefficient can be obtained when the entire cantilever beam is bent in whole. This does mean that at small bending angles, the maximum factor is 1.62×10^{-8} C/m, which is much closer

to the DFT calculation result of Xu *et al.*[31] and Hong and Vanderbilt.[35]

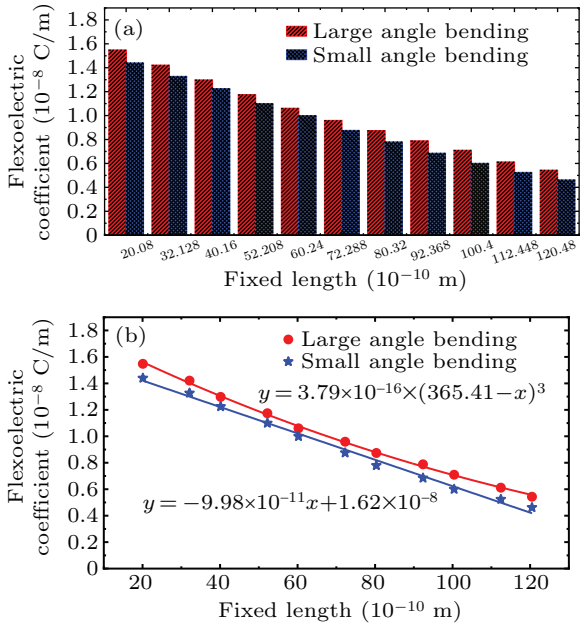


Fig. 8. Relationship between length of the fixed end and flexoelectric coefficient: (a) histogram of flexoelectric coefficient with different cantilever beam bendings for different fixed lengths, and (b) discrete data points denoting results of molecular dynamics simulations and the solid line referring to theoretical fit curve.

It can be seen from Fig. 8(b) that the nonlinear flexoelectric coefficient is slightly larger than the linear flexoelectric coefficient. However, the difference between the two does not seem to be very significant. A careful analysis of the physics is essential at this point. From the dimensional analysis of physics, the deflection δ is possible to obtain

$$\delta \approx \frac{F \cdot l^3}{Y \cdot I}, \tag{16}$$

where F is the externally applied force, Y is the Young's modulus, and I is moment of inertia. Suppose that the length of the fixed part is x, the following relationship can be obtained:

$$\mu \approx \frac{F \cdot P}{2Y \cdot I} \cdot (L-x)^3. \tag{17}$$

Experimentally, small angles are sometimes difficult to measure. When large angles of bending are considered, the nonlinear flexoelectric coefficient is much more accurate. So the above equation is used to fit the variable fixed length and the fitted result shows that the maximum flexoelectric coefficient of $BaTiO_3$ (BT) crystal is $\mu_{12} = 1.85 \times 10^{-8}$ C/m. This result is consistent with those reported by several researchers as listed in Table 5, the larger coefficient should come from the non-linear effects.

The experimental data yield larger coefficients for the flexoelectric effects, which should correlate with the nonlinear effects at a larger bending. From the preceding analysis, it linearly relate the polarization to the fixed length in the case of small angle bending, while in large angle bending the polarization satisfies a cubic proportional relationship with the fixed end length. This method provides a universal reference for predicting the maximum flexoelectric coefficient of many materials.

Table 5. Flexoelectric coefficients of $BaTiO_3$ and other materials from simulations and experiment.

Materials	Source	Longitudinal μ_{11} (C/m)	Transverse μ_{12} (C/m)	Shear μ_{14} (C/m)	Methods
$BaTiO_3$	this study	–	1.85×10^{-8}	–	MD
	Cross L E[8]	–	5×10^{-5}	–	experiment
	Maranganti R[10]	1.5×10^{-10}	-5.463×10^{-9}	-1.904×10^{-9}	rigid-ion model
	Xu T[31]	-3.6×10^{-10}	1.6×10^{-9}	-1.5×10^{-9}	DFT
	Hong J W	-3.7×10^{-10}[33]	-2.3×10^{-8}[35]	–	DFT
	Gharbi M[34]	–	4×10^{-6}	–	experiment
	Narvaez J[36]	–	2×10^{-7}	–	experiment
$Ba_{0.7}Ti_{0.3}O_3$	Kwon S R[37]	–	2.45×10^{-5}	–	experiment
NaCl	Askar A[38]	4.23×10^{-12}	-1.19×10^{-12}	-2.3×10^{-12}	lattice dynamics
BT-8BZT	Huang S J[39]	–	2.5×10^{-5}	–	experiment
PMN-PT	Narvaez J[40]	–	3.8×10^{-5}	–	experiment
$SrTiO_3$	Ponomareva I[41]	5.1×10^{-9}	3.3×10^{-9}	4.5×10^{-11}	DFT
$Ba_{0.67}Sr_{0.33}TiO_3$	Ma W H[42]	–	1×10^{-4}	–	experiment
$MAPbBr_3$	Shu L L[43]	–	2.4×10^{-5}	–	experiment
$MAPbCl_3$		–	3.3×10^{-5}	–	
Pt/BTO/Nb:STO	Huang S J[44]	–	$(2.87–4.18)\times10^{-4}$	–	experiment
PZT	Ma W H[45]	–	1.5×10^{-6}	–	experiment
PMN	Ma W H[9]	–	4×10^{-6}	–	experiment
$BaZrO_3$	Hong J W[11]	-1.9×10^{-10}	-2.1×10^{-10}	–	DFT
$PbTiO_3$		-0.2×10^{-9}	-0.25×10^{-9}	–	

Other flexoelectric materials such as $Ba_{0.7}Ti_{0.3}O_3$, $SrTiO_3$, $Ba_{0.67}Sr_{0.33}TiO_3$, NaCl, BT-8BZT, PMN-PT, and $MAPbBr_3$. are also included in Table 5. It can be seen that the experimental flexoelectric coefficients are usually 10^{-6} C/m–10^{-4} C/m, which is much larger than the theoretically calculated response (about 10^{-10} C/m–10^{-8} C/m). The discrepancy between theoretical result and experimental result may come from two reasons. Experimentally, the measured flexoelectric effect may be incorporated into the contribution of other effects, such as the piezoelectric effect or others. This requires a more ingenious experimental design to exclude the effects of other effects so as to accurately measure the flexoelectric coefficient. On the other hand, the current theoretical study is difficult to predict the proper flexoelectric effects. It requires the current theory to be modified or reconstructed to accurately predict the flexoelectric effects. Therefore, further studies should be carried out to accurately predict the flexoelectricity of condensed materials.

4. Conclusions and perspectives

First, the stability of the core–shell model in $BaTiO_3$ is verified by calculating the radial distribution functions at different temperatures. It is found that the core–shell potential model is effective and the structure of $BaTiO_3$ is stable in the temperature range of 10 K–150 K. Second, molecular dynamics method is used to study the phase transition temperature of $BaTiO_3$, and the obtained results are similar to experimental and theoretical calculations. It can give the correct phase transition temperatures. Simulated hysteresis loops of $BaTiO_3$ in the three directions [001], [110], and [111] demonstrate that anisotropy can have an important effect on the structure and motion of ferroelectric domain, which usually severely constrains the coercive field. Finally, the molecular dynamics method is used to predict the flexoelectric coefficient of $BaTiO_3$. From the theoretical analysis, it can be found that it linearly relate the polarization to the fixed length when the bent angle is small, and it satisfies a cubic proportional relationship with the fixed end length as the bending angle becomes larger.

Acknowledgements

We thank Xianglai Gan of Nanchang university for the illuminating and fruitful discussion. We also heartfeltly thank professor Shanming Ke for his help.

Project supported by the Natural Science Funds of Ningxia, China (Grant No. ZR1221) and the National Natural Science Foundation of China (Grant No. 11964027).

References

[1] Yan Y, Kim W G, Ma X T, Tegafaw T, Nguyen T M, Lee J M, Choi E J, Ahn H, Ha S H, Kim K, Kim J M, Kim H K, Oh J E, Shin D M and Hwang Y H 2021 *Nano Energy* **81** 105607
[2] Rojas E F, Faroughi S, Abdelkefi A and Park Y H 2021 *Appl. Energy* **288** 116611
[3] Su S, Huang H and Zhu Z H 2021 *Energy* **224** 120056
[4] Coy E 2020 *Measurement* **163** 107986
[5] Ke X Q, Deng Q and Yang S 2021 *Ceram Int.* **47** 4310
[6] Tagantsev A K 1986 *Phys. Rev. B* **34** 5883
[7] Ma W H and Cross L E 2001 *Appl. Phys. Lett.* **79** 4420
[8] Ma W and Cross L E 2006 *Appl. Phys. Lett.* **88** 232902
[9] Ma W H and Cross L E 2002 *Appl. Phys. Lett.* **81** 3440
[10] Maranganti R and Harma P 2009 *Phys. Rev. B* **80** 054109
[11] Hong J W and Vanderbilt D 2013 *Phys. Rev. B* **88** 174107
[12] Thompson A P, Aktulga H M, Berger R, Bolintineanu D S, Brown W M, Crozier P S, Veld P J, Kohlmeyer A, Moore S J, Nguyen T D, Shan R, Stevens M J, Tranchida J, Trott C and Plimpton S T 2022 *Comput. Phys. Commun.* **271** 108171
[13] Plimpton S 1995 *J. Comput. Phys.* **117** 1
[14] Mitchell P J, Fincham D 1993 *J. Phys.: Condens. Matter* **5** 1031
[15] Sepliarsky M, Asthagiri A, Phillpot S R, Stachiotti M G and Migoni R L 2005 *Curr. Opin. Solid State Mater.* **9** 107
[16] Boddu V, Endres F and Steinmann P 2017 *Sci. Rep.* **7** 806
[17] Goh W F, Khan S A and Yoon T L 2013 *Model Simul. Mater. Sci.* **21** 045001
[18] Leyva, Ruiz, Anglada-Rivera and Zayas 2012 *Revista Cubana de Química* **24** 266
[19] Karvounis A, Timpu F, Vogler-Neuling V V, Savo R and Grange R 2020 *Adv. Opt. Mater.* **8** 2001249
[20] Gonçalves L G V and Rino J P 2017 *Comput. Mater. Sci.* **130** 98
[21] Tinte S, Stachiotti M G, Phillpot S R, Sepliarsky M, Wolf D and Migoni R L 2004 *J. Phys. Condens Mater.* **16** 3495
[22] Lemanov V V, Smirnova E P, Syrnikov P P and Tarakanov E A 1996 *Phys. Rev. B* **54** 3151
[23] Merz W J 1949 *Phys. Rev.* **76** 1221
[24] Bell A J and Cross L E 1984 *Ferroelectrics* **59** 197
[25] Ma Z, Ma Y N, Chen Z P, Zheng F, Gao H, Liu H F and Chen H M 2018 *Ceram. Int.* **44** 4338
[26] Cross L E 2006 *J. Mater. Sci.* **41** 53
[27] Maranganti R and Sharma P 2009 *Phys. Rev. B* **80** 054109
[28] Pikin S A and Indenbom V L 1978 *Ferroelectrics* **20** 151
[29] Ma W and Cross L E 2005 *Appl. Phys. Lett.* **86** 072905
[30] Ma W H and Cross L E 2001 *Appl. Phys. Lett.* **78** 2920
[31] Xu T, Wang J, Shimada T and Kitamura T 2013 *J. Phys.: Condens. Matter* **25** 415901
[32] Abarca M E 2018 *Universitat Politècnica de Catalunya. Masters Thesis*
[33] Hong J W, Catalan G, Scott J F and Artacho E 2010 *J. Phys. Condens. Matter* **22** 112201
[34] Gharbi M, Sun Z H, Sharma P, White K and El-Borgi S 2011 *Int. J. Solids Struct.* **48** 249
[35] Hong J W and Vanderbilt D 2013 *Phys. Rev. B* **88** 174107
[36] Narvaez J, Saremi S, Hong J W, Stengel M and Catalan G 2015 *Phys. Rev. Lett.* **115** 037601
[37] Kwon S R, Huang W B, Shu L L, Yuan F G, Maria J P and Jiang X N 2014 *Appl. Phys. Lett.* **105** 142904
[38] Askar A, Lee P C Y and Cakmak A S 1970 *Phys. Rev. B* **1** 3525
[39] Huang S J, Kim T, Hou D, Cann D, Jones J L and Jiang X N 2017 *Appl. Phys. Lett.* **110** 222904
[40] Narvaez J and Catalan G 2014 *Appl. Phys. Lett.* **104** 162903
[41] Ponomareva I, Tagantsev A K and Bellaiche L 2012 *Phys. Rev. B* **85** 104101
[42] Ma W H and Cross L E 2002 *Appl. Phys. Lett.* **81** 3440
[43] Shu L L, Ke S M, Fei L F, Huang W B, Wang Z G, Gong J H, Jiang X N, Wang L, Li F, Lei S J, Rao Z G, Zhou Y B, Zheng R K, Yao X, Wang Y, Stenge M and Catalan G 2020 *Nat. Mater.* **19** 605
[44] Huang S J, Yau H M, Yu H, Qi L, So F, Dai J Y and Jiang X N 2018 *AIP Adv.* **8** 065321
[45] Ma W H and Cross L E 2003 *Appl. Phys. Lett.* **82** 3293